Proceedings of the 20th International Conference on Soil Mechanics and Geotechnical Engineering– Rahman and Jaksa (Eds)

Pile running problem and large deformation modelling

Pile Running Problème et modélisation de grande déformation

Yinghui Tian & M. J. Cassidy
Melbourne School of Engineering, The University of Melbourne, Australia

H. Zhao
School of Civil Engineering, Tianjin University, China

ABSTRACT: Steel pipe piles are widely used in offshore and coastal engineering to support platforms and bridges. A challenging issue for installing a long and heavy pile is the problem of 'pile running', which refers to the phenomenon of rapid penetration into the seabed under self-weight. Unexpected pile running can cause breakage of the harnessing wire connecting the pile hammer or over penetration of the pile into the seabed. Predicting the pile running process and ultimate penetration depth is challenging due to the large deformations involved. This paper utilises large deformation numerical modelling based on Coupled Euler-Lagrangian method to examine the pile running process. The Coupled Eulerian-Lagrangian method models the seabed soil as a Eulerian domain with fixed mesh nodes and with the soil material capable of flowing through the mesh. The pile is modelled as a Lagrangian object and the interaction between pile and soil is described using a general contact algorithm. After validation of the numerical method, engineering incidents reported offshore western India, the Richmond-San Rafael bridge and offshore China were retrospectively simulated. Good agreement with the field observations were obtained and the underlying mechanism of pile running has been interpreted. This provides a useful reference for offshore engineers to evaluate pile running.

KEYWORDS: Pile; running; layered soil; large deformation analysis.

1 INTRODUCTION

Large diameter and long pipe piles are one of the most common foundation types in offshore engineering. Fig. 1 shows a 158m long pipe pile used as the foundation for a jacket platform. Compared with the traditional practice requiring segmental splicing, a long pile fabricated with only one segment can significantly reduce installation time and thus avoid the problem of pile refusal upon restarting driving after splicing. Nevertheless, one challenging issue for a long pile with heavy weight is 'pile running' during installation. This terminology refers to the phenomena of uncontrollably rapid penetration of the pile into the seabed under self-weight. Unexpected pile running can cause breakage of the harnessing wire connecting the pile hammer, losing the hammer into sea water or over penetration of the pile into the seabed.

Figure 1. A 158m long pile.

Detailed reports and case studies of pile running have not been reported comprehensively in the literature, though it is not an uncommon design issue. Two main reasons may cause pile running of long piles. One is associated with the process of pile driving in carbonate soils with low shaft resistance caused by particle breakage along the pile (Brunning & Ishak 2012; Senders et al. 2013; Banimahd et al. 2017). The other is piling in layered soils where significant variation of pile base resistance can occur from layer to layer.

This paper addresses the issue of pile running in layered soil by reviewing several pile running incidents, where the seabed characterisation and parameters of the soil stratigraphy are presented. The numerical modelling of pile running is extremely challenging due to the large deformation of soil around the pile. Three-dimensional large deformation finite element analyses based on the Coupled Eulerian-Lagrangian (CEL) method were adopted in this paper, where a Coulomb pile-soil interaction model was used by accounting for the variation of pile-soil interface friction. Soil softening and rate effects were considered for clay soil layers. The successful predictions of pile running in this paper provides a useful tool to assess the possibility of pile running during the design of pile foundations.

2 LARGE DEFORMATION MODELLING

2.1 *CEL method*

The CEL method has been widely used to investigate large deformation problems of offshore structure installation such as spudcans, pipelines and anchors (Tho et al., 2012; Qiu et al., 2011; Hu et al., 2014; Hamann et al., 2015). In a CEL analysis, the spatial position of nodes of the Eulerian domain is fixed and materials (i.e. soils) are allowed to flow through the mesh, thus the mesh distortion problem can be avoided. An index of Eulerian Volume Fraction (EVF) is used to describe the proportion of elements occupied by the Eulerian material (soil). The interaction

between the Eulerian material and Lagrangian object (pile in this study) is modelled using a general contact based on a penalty contact algorithm (Dassault Systèmes, 2016).

2.2 *Key implementations in the modelling*

2.2.1 *Softening and rate effect of clay soil*

The strain rate effect caused by rapid penetration and the softening effect caused by soil remoulding influence the shear strength of the clay. As recommended by Einav & Randolph (2005) the undrained shear strength can be updated as:

$$s_u = s_{u0}\left[\delta_{rem} + (1-\delta_{rem})e^{-3\xi/\xi_{95}}\right]\left[1+\mu\log\left(\frac{|\dot{\gamma}_{max}|}{\dot{\gamma}_{ref}}\right)\right] \quad (1)$$

where s_{u0} is the original shear strength; δ_{rem} is the ratio between the fully remoulded and the original undrained shear strength, which is the inverse of soil sensitivity S_t; ξ is the accumulated absolute plastic shear strain and ξ_{95} is the value of ξ for 95% shear strength degradation (ξ_{95} has typical values ranging 10-30); μ indicates the rate of undrained shear strength increase per decade, ranging within 0.05-0.2 (Randolph et al., 2005; Zhou et al., 2007; Kim et al., 2015). $\dot{\gamma}_{ref}$ is the reference strain rate, and the maximum shear strain rate defined as:

$$\dot{\gamma}_{\max} = \frac{\Delta\varepsilon_1 - \Delta\varepsilon_3}{\Delta t} \quad (2)$$

where $\Delta\varepsilon_1$ and $\Delta\varepsilon_3$ are the cumulative major and minor principal strains over the incremental time period Δt. This model was implemented into the coupled Eulerain-Lagrangian method in this study to describe the shear strength change.

2.2.2 *Pile-soil interaction and the softening of shaft skin friction*

For the large deformation during penetration of pipe piles, the accuracy of the friction at the pile-soil interface directly affects the penetration resistance, which in turn affects the final depth of pile running. The CEL method uses the Coulomb friction model to calculate friction allowing a maximum shear strength τ_{max} to define the shear behavior of the pile-soil interface. In this paper, the maximum shear strength τ_{max} at the pile-soil interface uses $\tau_{max} = \alpha s_u$ for clay layer following API (2006), where the friction ratio α was taken as the inverse of the soil sensitivity (S_t) to simulate that the soil around the pile is completely remolded. For sand, τ_{max} can be estimated as:

$$\tau_{max} = K\sigma'_v \tan\delta \quad (3)$$

where σ'_v is the effective overburden stress at a certain depth in the soil; K is the lateral earth pressure coefficient with an estimation of $K=\mu/(1-\mu)$, where μ is the Poisson's ratio and $\mu = 0.35$ is used in this paper; δ is the pile-soil friction angle.

3 CASE STUDY

3.1 *Pile running incident offshore Western India*

A jacket platform in western India was built in a water depth of 30m. At the beginning of piling, four main piles of the jacket ran under their own weight, and the running depth reached 33m (Bhowal & Nanda, 2000). The pile length was 78m and the pile wall thickness varied within 32~38mm, where the wall thickness around the pile toe was 38mm. The pile diameter was 1.829m. See Table 1 for the soil layer stratigraphy and soil conditions.

Table 1 shows the soil conditions where nine layers of clay and sand were present. The numerical model was created based on this data, but with only the top six layers (0-58m) included, as the pile running incident occurred within this range. Fig. 2 shows the finite element model. In the Mohr-Coulomb model assumed the friction angle for clay and the cohesion for sand layer were both zero. Poisson's ratio of clay was taken as 0.49, and Young's modulus considered as $E=500s_u$. For sand layers, Young's modulus was taken as E=35MPa and Poisson's ratio μ=0.35.

Table 1. Soil parameters (The western India)

Layers	*Depth* (m)	s_u (kPa)	φ(°)
Very soft clay	0-8	2-7	-
Soft clay	8-18	7-19	-
Loose sand	18-25.5	-	20
Firm clay	25.5-48	26-56	-
Medium sand	48-50	-	25
Medium sand	50-58	-	30
Very stiff clay	58-60	160	-
Stiff clay	60-61	60	-
Dense sand	61-79.3	-	35

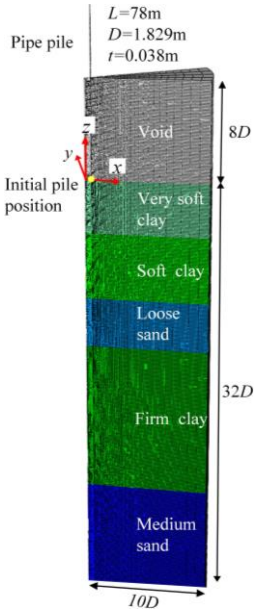

Figure 2. Numerical model for western India incident.

Fig. 3 is the pile running simulation result for the offshore western India incident. The numerical prediction of pile running depth was 35.1m, where the actual pile running depth was 33.0m. It can be seen from the pile running velocity-depth curve in Fig. 3a that in the top clay layers (0~18m), the pile ran quickly from the mud surface, and the pile speed continued to increase until it encountered the layer of sand. In the sand layer, the pile reached the peak speed of 15.7m/s and decelerated. When the pile entered the underneath clay layer, the pile continued to decelerate and stopped at 35.1m in the firm clay layer.

From the total penetration resistance-depth curve in Fig. 3b, it can be seen that as the pile penetrated downward from the mud surface, the total penetration resistance started to increase slowly

from zero. In the layer of clay, the total penetration resistance was continuously increasing, but it was much smaller than the weight of the pile. When the pile approached and entered the sand layer, the penetration resistance increased rapidly. There was a peak point of the penetration resistance, which happened later than the maximum speed of the pile. When the pile penetrated into the clay layer underneath the sand layer, the penetration resistance of the pile dropped rapidly, but it was still greater than the weight of the pile. Thus the pile slowed down and eventually stopped in the clay layer.

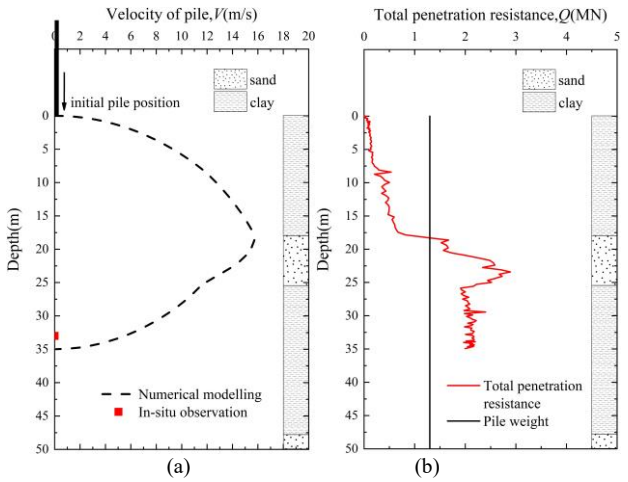

Figure 3. The pile running simulation of the western India incident: (a) Velocity-depth curve and (b) Total penetration resistance-depth curve.

Further analysis of the pile base resistance Q_b and pile shaft resistance Q_s (including outer shaft resistance $Q_{s,outer}$, the inner shaft resistance $Q_{s,inner}$) is shown in Fig. 4. The outer shaft resistance $Q_{s,outer}$ increased monotonically with depth while the inner shaft resistance $Q_{s,inner}$ peaked in the sand layer and reduced afterwards. This is due to partial soil plugging with a sand layer plug formed inside the pipe pile. In the fourth layer of the firm clay, the outer shaft resistance was greater than the inner resistance and the base resistance. Compared with the pile base resistance, the pile shaft resistance became the main contributor to stop pile running in the fourth layer of firm clay.

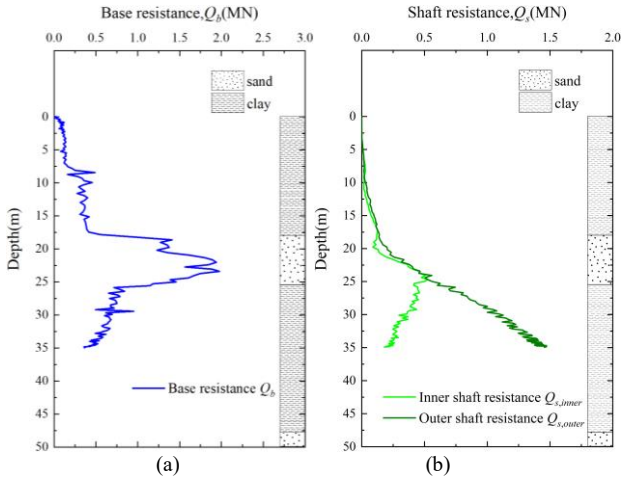

Figure 4. The penetration resistance of pile running of the western India: (a) Base resistance-depth curve and (b) Shaft resistance-depth curve.

3.2 *The Richmond-San Rafael bridge incident*

The Richmond-San Rafael Bridge is about 7km long and the water depth 21m. There are 4 large diameter pipe piles distributed under each pier, where the pile outer diameter is 3.20-4.11m and wall thickness 38-57mm. During the reinforcement of the bridge, pile running incidents occurred (Dover & Davidson, 2007). Among them, No. 47 pier was selected for the research in this paper. The four pipe piles used for No. 47 pier are named P47-1, P47-2, P47-3 and P47-4. The pipe piles have an outer diameter of 4.11m, a wall thickness of 57mm, and a pile weight of 278t. The soil parameters in this area are shown in Table 2.

Table 2. The design parameters of soils (The Richmond-San Rafael bridge)

Layers	*Depth*(m)	s_u (kPa)	φ(°)
Top Veneer	0-6	0	15-20
Young Bay Mud	0-36	4-60	-
Merritt Sand and San Antonio Formation	0-10	45-90	25-40
Alameda Formation or Older Alluvium	0-18	120+	-

The numerical model setup is similar as Fig. 2 and thus is omitted. The analysis results were compared with the measured pile running depth of the four piles, as shown in Fig. 5. The numerically predicted depth was 42.7m, and the maximum speed of the slide pile was 14.2m/s. The actual running depth was between 35m and 38m. No further detailed soil layer information is available and the predicted depth is regarded to have a good agreement within an acceptable range. It can be seen from the pile velocity-depth curve in Fig. 5a that in the thick clay layer, the pile started to run quickly from the mud surface. At the middle position of the thick clay layer, the pile speed slowed down. The acceleration and deceleration of pile occurred in the thick clay layer. Eventually, the pile stopped in the lower sand layer with the rapid increase of base resistance.

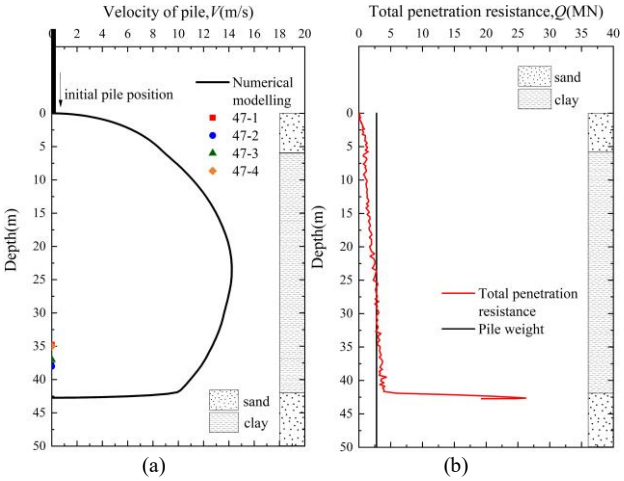

Figure 5. The pile running simulation of the Richmond-San Rafael bridge: (a) Velocity-depth curve and (b) Total penetration resistance-depth curve.

From the total penetration resistance-depth curve of the pile in Fig. 5b, it can be seen that as the pile penetrated downward from the mud surface, the total penetration resistance started to increase slowly from zero. When the pile penetrated from the first layer of sandy soil into the thick clay layer below, the total penetration resistance was slightly reduced, but it had little effect

on the increase trend of the entire penetration resistance. When the pile penetrated into the middle depth of the thick clay, the penetration resistance of the pile became slightly greater than the weight of the pile and the penetration speed decreased slowly. When the pile penetrated into the lower sand layer, the penetration resistance of the pile increased rapidly, causing the pile speed to decelerate quickly, and finally stopped.

Fig. 6 shows the pile base resistance and shaft resistance during the pile penetration process. In the first layer of sand, the pile base resistance increased from zero, while the pile penetration in the thick clay layer, the pile base resistance stabilized. However, the continuous increase of pile shaft friction caused the total resistance of the pile to be greater than the weight of the pile, which caused the pile to decelerate in the thick clay layer. When the pile entered the sandy soil layer, the pile base resistance increased rapidly, but the pile shaft resistance did not change significantly, and still maintained an increasing trend. It is proved that the main contribution of the increase of the total penetration resistance of the pile in the sand layer comes from the pile base resistance, which caused the rapid decline of the pile speed and finally led to the end of the pile running.

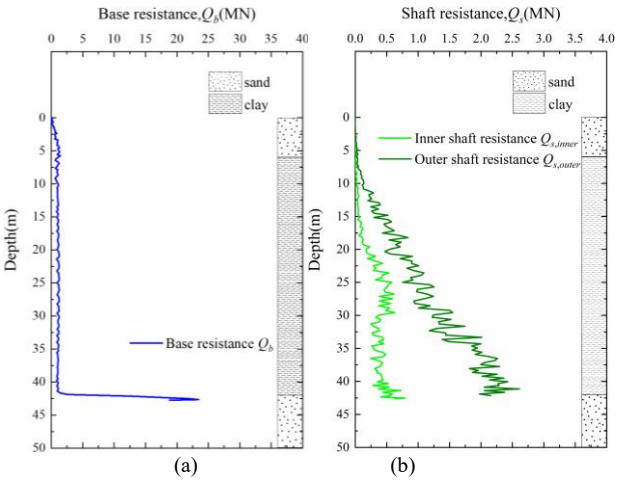

Figure 6. The penetration resistance of pile running of the Richmond-San Rafael bridge: (a) Base resistance-depth curve and (b) Shaft resistance-depth curve.

3.3 *Offshore China incident*

An offshore oil jacket platform in the East China Sea encountered a pile running problem during the construction phase (Li et al., 2014). The jacket platform was installed in an average water depth of 84.1m and had 12 large diameter steel pipe piles. The diameter of the piles was 2.438 and the wall thickness 0.045-0.08m. The pile length was 118.5m with each pile weighing 434.9t and the final penetration depth was 96m. The file observation of the range of the pile running was between 38m and 55m. According to the geological conditions of the area where the jacket platform is located, 15 soil layers are present, which mainly include silty fine sand, sandy silt sand and silty clay. Table 3 details the engineering design parameters of the soil.

The analysis results of pile running of the offshore China incident (with the pile initially embedded at 38m deep) were compared with the actual measured hammer piling records, as shown in Fig. 7. From the hammering records, it can be seen that the range of pile running was 38m to 55m. The prediction range of the pile running was in good agreement with the actual measurement range (Fig. 7b). Both acceleration and deceleration of the pile running occurred in the thick clay layer. In the middle of the layer, there was a maximum pile velocity 6.5m/s at 45m, where total penetration resistance began to exceed the pile weight (Fig. 7c). The pile speed in the clay layer developed gradually as there was no abrupt layer interface existed.

Table 3. The design parameters of soils (Offshore China)

Layers	*Depth*(m)	s_u(kPa)	γ(kN/m^3)	φ(°)	S_t(°)
Silty Sand	0-1.8	-	19.2	22.5	-
Sand	1.8-3.3	-	19.0	30	-
Silty Clay	3.3-8.0	15	18.5	-	3.5
Silty Clay	8.0-13.0	30	17.2	-	3.5
Silty Sand	13.0-19.5	-	19.0	30	-
Silty Sand	19.5-24.4	-	19.5	30	-
Sandy Silt, fine sand	24.4-38.0	-	18.6	30	-
Silty Clay	38.0-39.2	60	18.4	-	3.5
Silty Clay and Silt	39.2-53.0	110	18.8	-	3.5
Sandy Silt	53.0-55.2	-	19.0	35	-
Silty Clay	55.2-57.6	200	20.0	-	3.5
Sandy Silt, fine sand	57.6-64.2	-	18.9	35	-
Silty Clay and Silt	64.2-72.8	120	19.2	-	3.0
Sandy Silt	72.8-81.0	-	19.4	35	-

Fig. 8a showed the pile base resistance was relatively small when pile running started because there was a thin soft layer of silty clay (38~39.2m). When reaching the harder clay layer below (39.2~53m), the pile base resistance began to increase and gradually stabilized until the pile tip touched the lower sand layer, where the pile base resistance increased significantly. Fig. 8b showed the pile outer and inner shaft resistance in the clay layer increased constantly. When pile came to contact with the sandy soil layer, the inner shaft resistance decreased due to the partially forming of soil plug.

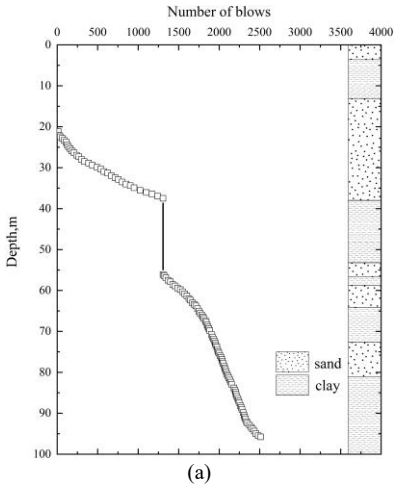

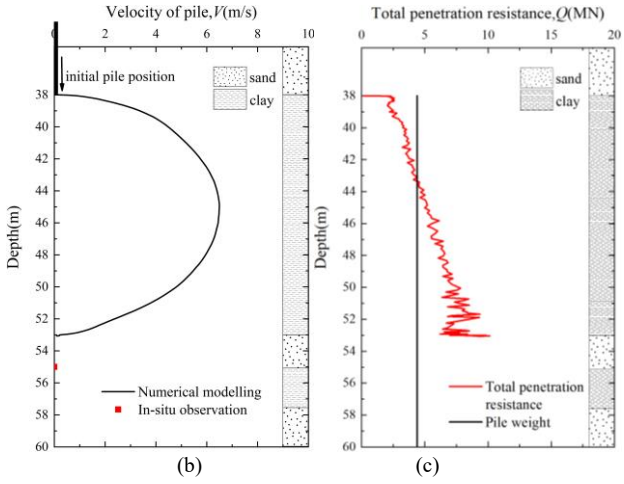

Figure 7. The pile running simulation of Offshore China: (a) Pile driving record, (b) Velocity-depth curve and (c) Total penetration resistance-depth curve.

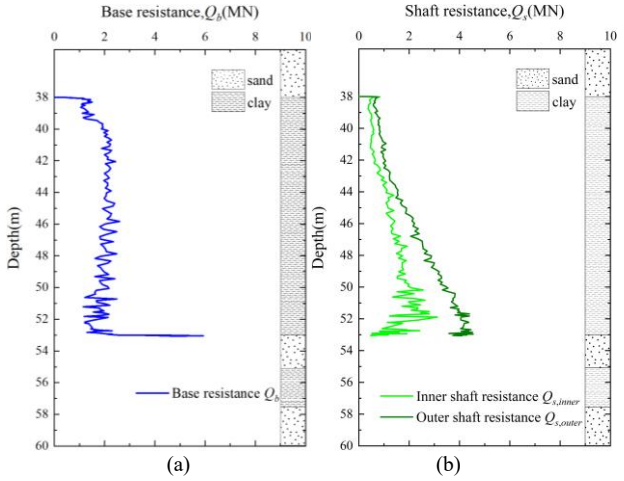

Figure 8. The penetration resistance of pile running of Offshore China: (a) Base resistance-depth curve and (b) Shaft resistance-depth curve.

4 CONCLUSIONS

This paper reviewed three pile running incidents and adopted large deformation analysis to retrospectively model the pile running process. The main conclusions of this study include:

- The soil strength degradation was accounted from two aspects. One is the degradation of interface friction between pile and soil to s_u/S_t, which led to a predicted running displacement of 17.5% more. The other is the strain softening and strain rate of clay layers. Considering strain softening predicted a 3.7% extra running displacement and considering strain rate effect led to 0.9% less. Considering both strain softening and rate effect ended up in 3.1% extra running displacement.
- The drastic change of pile base resistance between adjacent soil layers is a main reason for uncontrollable pile running in layered soils.
- The contribution from pile base resistance in sandy soil substantially causes pile running to stop.
- Due to the accumulation of pile shaft resistance, pile running can also gradually stop in the thick clay layer.
- The evolution of inner shaft resistance is greatly influenced by layered soils, where the soil plug can partially form when entering sandy layers.

5 ACKNOWLEDGEMENTS

The first author acknowledges the Australian Future Fellowship (FT200100457) for the support of conducting frontier research in offshore geotechnics.

6 REFERENCES

American Petroleum Institute. 2006. Recommended Practice for Planning, Designing and Constructing Fixed Offshore Platforms (RP 2A-WSD), Washington DC: API.

Banimahd, M., Chow, F., Tyler, S., Senders, M. and Stewart-Wynne, R. 2017. Hold-Back Anchor Piles with Free Fall Potential on the Australian North-West Shelf. Offshore Site Investigation Geotechnics 8th International Conference Proceedings, 1198–1205.

Bhowal, S. and Nanda, A. 2000. Rundown of offshore piles. 2000. International Conference on Offshore and Nearshore Geotechnical Engineering. Oxford & IBH, New Delhi(India): 81-86.

Brunning, P., and Ishak, B. 2012. Pile driving in Carbonate Soils and Rock of the Australian North West Shelf - a Case Study, 7th Int. Offshore Site Investigation and Geotechnics Conference, London, UK, 489-495.

Dassault Systèmes. 2016. Abaqus Analysis User's Manual. SIMULIA, Providence, RI.

Dover, A.R. and Davidson, J. 2007. Large Diameter Steel Pipe Piles Running Under Self Weight in Soft Clay: Predicted vs. Observed Behavior-Richmond-San Rafael Bridge Seismic Retrofit. Ports 2007, 1-10.

Einav, I. and Randolph, M.F. 2005. Combining Upper Bound and Strain Path Methods for Evaluating Penetration Resistance. International Journal for Numerical Methods in Engineering, 63(14):1991-2016.

Hamann, T., Qiu, G., Grabe and Jürgen. 2015. Application of a Coupled Eulerian-Lagrangian Approach on Pile Installation Problems under Partially Drained Conditions. Computers & Geotechnics, 63:279-290.

Hu, P., Wang, D., Cassidy, M.J. and Stanier, S. A. 2014. Predicting the Resistance Profile of a Spudcan Penetrating Sand Overlying Clay. Canadian Geotechnical Journal, 51(10), 1151-1164.

Kim, Y.H., Hossain, M.S., Wang, D. and Randolph, M.F. 2015. Numerical Investigation of Dynamic Installation of Torpedo Anchors in Clay. Ocean Engineering, 108, 820-832.

Li, S., Wang, H., Pu, Y., Sun, Z., Fan, Z. and Han, L. 2014. Influence of Pile Sinking On Pile Capacity During Pile Driving On Offshore Platforms. China Earthq. Eng. J. 36,462–467, (in Chinese).

O'Loughlin, C.D., Gaudin, C., Randolph, M.F. and Richardson, M.D. 2013. Penetration of Dynamically Installed Anchors in Clay. Géotechnique, 63(11), 909-919.

Qiu, G., Henke, S. and Jürgen Grabe. 2011. Application of a Coupled Eulerian–Lagrangian Approach on Geomechanical Problems Involving Large Deformations. Computers and Geotechnics, 38(1), 30-39.

Senders, M., Banimahd, M., Zhang, T. and Lane, A. 2013. Piled Foundations on the North West Shelf, Australian Geomechanics, 48(4), 149-160.

Randolph, M.F., Leong, E.C. and Houlsby, G.T. 1991. One-dimensional Analysis of Soil Plugs in Pipe Piles. Géotechnique, 41(4), 587–598.

Randolph, M.F., Cassidy, M.J., Gourvenec S. and Erbrich C. Challenges of Offshore Geotechnical Engineering. In: Proc. 16th International Conference on Soil Mechanics and Geotechnical Engineering, Osaka. 2005, pp. 123–76.

Tho, K.K., Leung, C.F., Chow, Y.K. and Swaddiwudhipong, S. 2012. Eulerian Finite-Element Technique for Analysis of Jack-up Spudcan Penetration. International Journal of Geomechanics, 12(1), 64-73.

Zhou, H. and Randolph, M.F. 2007. Computational Techniques and Shear Band Development for Cylindrical and Spherical Penetrometers in Strain-Softening Clay. International Journal of Geomechanics, 7(4), 287-295.